

Enhanced transmission induced by embedded graphene in periodic, quasiperiodic, and random photonic crystals 1

ABHISHEK PADHY,¹  RAHUL BANDYOPADHYAY,¹ CARLOS H. COSTA,²
CLAUDIONOR G. BEZERRA,³ AND CHITTARANJAN NAYAK^{1,*} 

¹Department of Electronics and Communication Engineering, College of Engineering and Technology, SRM Institute of Science and Technology, SRM Nagar, Kattankulathur, Kanchipuram, Chennai, TN 603203, India

²Universidade Federal do Ceará, Campus Avançado de Russas, 62900-000, Russas-CE, Brazil

³Departamento de Física Teórica e Experimental, Universidade Federal do Rio Grande do Norte, Natal-RN 59078-900, Brazil

*Corresponding author: 83chittaranjan@gmail.com

Received 8 July 2020; revised 13 October 2020; accepted 15 October 2020; posted 16 October 2020 (Doc. ID 402357); published 0 MONTH 0000

The study of photonic crystals, artificial materials whose dielectric properties can be tailored according to the stacking of their constituents, remains an attractive research field, and it is the basis of photonic devices based on the generation, processing, and storage of photons. In this paper, we employ a transfer-matrix treatment to study the propagation of light waves in periodic, quasiperiodic (Fibonacci, Octonacci, and Dodecanacci), and random dielectric multilayers with graphene embedded. The structures considered here are composed of two building blocks, silicon dioxide (building block $A = \text{SiO}_2$) and titanium dioxide (building block $B = \text{TiO}_2$). We calculate their transmission spectra as a function of incident angle θ and reduced frequency Ω . Our main goal is to investigate the enhancement of the transmission due to the presence of graphene. In particular, we show that bandgap regions become passband regions when graphene is embedded in the optical multilayers. More specifically, for a range of the incident angle θ and reduced frequency Ω , the PCs with graphene embedded display an unexpected property: the electromagnetic radiation is transmitted mainly through the multilayers and not reflected or absorbed as expected for large structures. © 2020 Optical Society of America

<https://doi.org/10.1364/JOSAB.402357>

1. INTRODUCTION

The study of photonic crystals (PCs) started in 1987 with the independent seminal works of E. Yablonovitch [1] and S. John [2]. Those authors investigated the capability of semiconductor materials to guide and confine the propagation of light. PCs may be defined as structures consisting of alternating layers of two or more different dielectric materials, so that the artificially synthesized structure as a whole presents a spatially periodic permittivity function [3]. In recent years, a lot of research effort has been made towards the understanding and applications of PCs, concerning fabrication [4], prisms [5], lenses [6–9], filters [10,11], photonic quasiperiodic fibers (PQFs) [12–18], sensors [19], metasurfaces [20], surface waves [21], etc. Among all very interesting properties presented by PCs, one in particular makes these systems excellent options for technological applications and attractive objects of research: the emergence of frequency regions, named photonic bandgaps (PBGs), for which there is no emission or propagation of electromagnetic waves through the structure [22,23]. As a consequence, PCs work as high

reflectivity mirrors [24]. Usually the most common way for the formation of a PBG is Bragg scattering (conventional PBG) because it can occur in any photonic system [25]. However, PBGs can also be formed by the zero average refraction index ($\bar{n} = 0$ PBG) or phase conditions ($\bar{\phi} = 0$ PBG), for example, in left-handed materials (LHMs) [26]. Finally, when the PC presents a surface optical conductivity, a PBG can emerge as well. For instance, one can observe a graphene induced PBG (GIPBG) in PCs with embedded graphene [27].

Parallel to these developments in the field of PCs, the properties of a special and interesting class of structures, first discovered by Shechtman *et al.* [28] in 1984 and known as quasiperiodic crystals or quasicrystals (QCs), have been also widely investigated. One of the most important reasons is that they can be defined as an intermediate state between an ordered crystal (their definition and construction follow purely deterministic rules) and a disordered solid (many of their physical properties exhibit an erratic-like appearance) [29,30]. Hence, QCs present forbidden symmetries by classical crystal rules and long-range

correlation order [31]. When the alternating layers composing the PC are arranged according to a quasiperiodic sequence (with a well-defined mathematical substitution rule), so that the constituent dielectric function varies quasiperiodically, we have the so-called one-dimensional (1D) photonic QCs (1DPQCs) [32,33]. On the other hand, if the alternating layers composing the PC are arranged in a random fashion, for example, by following some probability function such as a Gaussian distribution [34,35], we have a 1D random PC (1DRPC), for which disorder-induced localization, delocalization, and inter-transition effects can be observed [36,37].

Graphene, the two-dimensional allotropic form of the carbon where atoms with sp^2 hybridization are strongly and densely attached creating a planar hexagonal crystalline lattice, has been hailed by many as the new silicon of the 21st century. This material is nearly 200 times stronger than steel, flexible, good for light absorption, and highly conductive to heat and electricity. With those remarkable physical properties, graphene is currently in the scientific limelight not only for possessing tremendous technological potential but also for having opened several avenues of basic science exploration [38,39]. Recently, a new and interesting research field, called *graphene nanophotonics* (GN) [40,41], has emerged. GN deals with optical systems in which graphene is integrated in the structure under investigation, usually with materials that operate in the terahertz frequency region [42]. In particular, 1D graphene-based PCs and PQCs have attracted interest from researchers because they are highly suitable for terahertz bandgap engineering applications [27].

In the present work, we intend to investigate more deeply the effects of inserting graphene at the interfaces of two different—non-dispersive and non-magnetic—dielectric layers (labeled as *A* and *B*) in 1D PCs (1DPCs). The structures were numerically investigated by employing the powerful transfer-matrix method (TMM), which simplifies the algebra [27,43]. The optical multilayers considered in this work are spatially arranged according to a periodic sequence, quasiperiodic sequences (such as Fibonacci [34], Octonacci [44], and Dodecanacci [45]), and also random sequences [46]. One should remark that, unlike what was done in previous works, we choose some specific generations for each sequence (periodic, quasiperiodic, or random) to obtain similar multilayer sizes [34,47]. Later, we give more details about the structures considered here.

This work is organized as follows. In Section 2, we present the physical model based on the TMM to solve the Maxwell's equations for electromagnetic waves in 1D graphene-based PCs. The physical parameters considered here as well as the numerical results are presented and discussed in detail in Section 3. Finally, our findings are summarized in Section 4.

2. PHYSICAL MODEL AND TRANSFER-MATRIX METHOD

The materials considered in this work are silicon dioxide (SiO_2), denoted by *A*, titanium dioxide (TiO_2), denoted by *B*, vacuum, denoted by *C*, and graphene, represented by its optical conductivity σ_g . The system is schematically presented in Fig. 1, where we present a periodic 1DPC consisting of alternating unit cells $|A|B$ juxtaposed to form the periodic finite array $|A|B|A|B|\dots|A|B|$. This array is surrounded by a

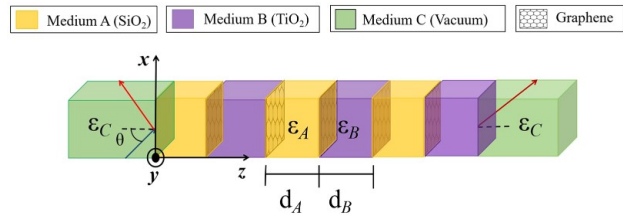


Fig. 1. Schematic representation of the 1DPC showing slabs *A* and *B*, incident and emergent media *C*, and graphene at the $A|B$ and $B|A$ interfaces.

semi-infinite media *C*, which is considered to be vacuum. The physical parameters of the optical media are the thicknesses (d_A and d_B) and dielectric permittivities (ϵ_A , ϵ_B , and ϵ_C).

The graphene embedded at the interfaces is modeled by a frequency-dependent conductivity $\sigma_g(\omega)$ composed of two contributions: (i) the intraband $\sigma_g^{\text{intra}}(\omega)$ (related to the scattering from phonons, electrons, and impurities); and (ii) the interband $\sigma_g^{\text{inter}}(\omega)$ (related to the electron–hole recombination) [48]. The explicit form of the graphene's surface conductivity is given by [49]

$$\sigma_g(\omega) = \sigma_g^{\text{intra}}(\omega) + \sigma_g^{\text{inter}}(\omega), \quad (1)$$

with

$$\sigma_g^{\text{intra}}(\omega) = i \frac{e^2}{\pi \hbar (\hbar \omega + i \Gamma)} \left\{ \mu_c + 2k_B T_K \ln \left[e^{(-\mu_c/k_B T_K)} + 1 \right] \right\} \quad (2)$$

and

$$\sigma_g^{\text{inter}}(\omega) = i \frac{e^2}{4\pi \hbar} \ln \left[\frac{2|\mu_c| - (\hbar \omega + i \Gamma)}{2|\mu_c| + (\hbar \omega + i \Gamma)} \right]. \quad (3)$$

Here e is the electronic charge, \hbar is the Planck's constant, k_B is the Boltzmann's constant, T_K is the temperature in Kelvin, Γ is the damping constant of graphene, and μ_c is the chemical potential (which can be controlled by the gate voltage). It is known from the literature that for $\hbar \omega$ much smaller than the chosen chemical potential, the interband contribution is negligible [48]. As a consequence, the light propagation will be more affected by the presence of graphene in the low frequency region, as was shown by Costa *et al.* [27].

A quasiperiodic structure can be experimentally constructed by juxtaposing two building blocks *A* and *B* following Fibonacci, Octonacci, and Dodecanacci sequences (see Ref. [50]). A Fibonacci sequence S_N is generated by appending the $N-2$ sequence to the $N-1$ one, i.e., $S_N = S_{N-1}S_{N-2}$ ($N \geq 2$). This construction algorithm requires initial conditions chosen as $S_0 = B$ and $S_1 = A$. The Octonacci sequence grows in such a way that its N th stage is iteratively given by the rule $S_N = S_{N-1}S_{N-2}S_{N-1}$, for $N \geq 3$, with $S_1 = A$ and $S_2 = B$. Finally, the N th generation of the Dodecanacci sequence can be iteratively obtained by the rule $S_N = (AS_{N-2}S_{N-1})^2 S_{N-1}$, for $N \geq 3$, with $S_1 = AAB$ and $S_2 = (AS_1)^2 S_1$. Figure 2 schematically illustrates the inflation rules of the quasiperiodic sequences considered here.

Here we have chosen periodic, quasiperiodic, and random structures with similar sizes for comparison purposes (around 600 slabs), the 14th Fibonacci generation (610 slabs), the ninth

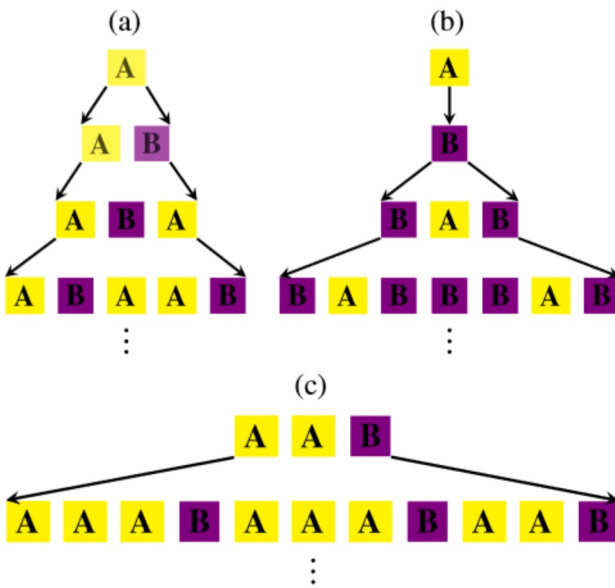


Fig. 2. Schematic illustration of the inflation rules for (a) Fibonacci, (b) Octonacci, and (c) Dodecanacci sequences.

Table 1. 1D Structures Considered in this Work

Name of the Sequence	Generation Number	Number of Layers
Periodic	–	600
Fibonacci	14	610
Octonacci	9	577
Dodecanacci	5	571
Random	–	600

Octonacci generation (577 slabs), and the fifth Dodecanacci generation (571 slabs), as summarized in Table 1. Regarding the periodic structure, the unit cell is repeated 300 times so that we get a structure with equivalent size, i.e., 600 slabs. For the random sequence, we use a random number generator function that chooses between two letters, *A* and *B*, and create a chain with 600 of these letters, considering a given probability of occurrence of the letter *A*, $p(A)$. For each value of $p(A)$, we consider four random sequences, which has been found to be a reasonable minimum quantity to obtain reliable conclusions.

We consider that a transverse electric (TE or *s*) or magnetic (TM or *p*) polarized monochromatic electromagnetic wave, traveling from left to the right in vacuum with angular frequency ω and wave-vector $\vec{k} = (k_x, k_z)$, obliquely reaches the photonic multilayer (distributed along *z* direction) at an angle θ from the normal (see Fig. 1). For the multilayer system considered here, whose unit cell is repeated n times, the transfer-matrix M_n that relates the amplitude of the electromagnetic wave at the interfaces is given by [27]

$$M_n = (M_A M_B)^n = \left(\prod M_j \right)^n, \quad (4)$$

with

$$M_j^{TE}(d_j, \omega)$$

$$= \begin{bmatrix} \cos(k_{sj}d_j) & \left(\frac{i}{q_j}\right) \sin(k_{sj}d_j) \\ \sigma_g \cos(k_{sj}d_j) + iq_j \sin(k_{sj}d_j) \cos(k_{sj}d_j) + \left(\frac{i\sigma_g}{q_j}\right) \sin(k_{sj}d_j) \end{bmatrix} \quad (5)$$

and

$$M_j^{TM}(d_j, \omega)$$

$$= \begin{bmatrix} \cos(k_{sj}d_j) - i\sigma_g q_j \sin(k_{sj}d_j) & -\sigma_g \cos(k_{sj}d_j) + \left(\frac{i}{q_j}\right) \sin(k_{sj}d_j) \\ iq_j \sin(k_{sj}d_j) & \cos(k_{sj}d_j) \end{bmatrix}. \quad (6)$$

Here $q_j = -\frac{k_{sj}}{\omega\mu_0}$ (for TE waves), and $q_j = \frac{k_{sj}}{\omega\varepsilon_0\varepsilon_j}$ (for TM waves). Also, k_{sj} is the *z* component of the wave-vector within medium *j* (*j* = *A* or *B*), which is given by

$$k_{sj} = \begin{cases} [\varepsilon_j(\omega/c)^2 - k_{xC}^2]^{1/2}, & \text{for } \varepsilon_j(\omega/c)^2 \geq k_{xC}^2, \\ i[k_{xC}^2 - \varepsilon_j(\omega/c)^2]^{1/2}, & \text{for } \varepsilon_j(\omega/c)^2 < k_{xC}^2, \end{cases} \quad (7)$$

where ε_j is the dielectric constant of medium *j*, *c* is the speed of light in vacuum, and k_{xC} is the *x* component of the incoming wave-vector.

It is known from the literature that the coefficients of transmission *T*, reflection *R*, and absorption *A* are obtained from the elements of the transfer-matrix M_n , which are given by [49]

$$T = \left| \frac{2q_C}{q_C M_{11} + q_C M_{22} - M_{21} + q_C^2 M_{12}} \right|^2, \quad (8)$$

$$R = \left| \frac{q_C M_{11} - q_C M_{22} - M_{21} + q_C^2 M_{12}}{q_C M_{11} + q_C M_{22} - M_{21} + q_C^2 M_{12}} \right|^2, \quad (9)$$

and

$$A = 1 - T - R. \quad (10)$$

Here M_{ij} are the elements of the transfer-matrix M_n , and q_0 , q_C are the parameters of the incoming and outgoing media *C*.

3. NUMERICAL RESULTS AND DISCUSSION

In this section, we present the numerical results and discussion concerning our investigation. The physical parameters considered in the numerical simulations are: the refraction indices and dielectric constants $n_A = \sqrt{\varepsilon_A} = 1.45$, $n_B = \sqrt{\varepsilon_B} = 2.30$, and $n_C = \sqrt{\varepsilon_C} = 1$; the thicknesses $d_A = 10.34 \mu\text{m}$ and $d_B = 6.52 \mu\text{m}$; the graphene's chemical potential $\mu_c = 0.2 \text{ eV}$; and temperature $T_K = 300 \text{ K}$. Here we take the graphene's damping constant $\Gamma = 0 \text{ eV}$ because it does not substantially affect the position or width of the PBGs, which is the aim of our work. In fact, it only qualitatively changes the probability of transmission [49]. It is important to mention that the thicknesses were calculated considering the quarter-wavelength condition of $d_j = \lambda_0/4n_j$ (*j* = *A* or *B*), such that $n_A d_A = n_B d_B$. Also, λ_0 is the central wavelength, and the results are given in terms of the reduced frequency defined as

$\Omega = \omega/\omega_0$, where $\omega_0 = 2\pi c/\lambda_0 \approx 31.4 \text{ rad} \cdot \text{THz}$ for a central wavelength $\lambda_0 = 60 \mu\text{m}$, chosen so that both dielectrics behave as non-dispersive media. We also remark that we have chosen a large number of slabs, around 600 slabs, to guarantee that the transmission spectra of the finite structures correspond to the dispersion relation of the infinite structures, as was investigated by Costa and Vasconcelos [51], where it was shown that, as the system grows up, the unit cell needs to be repeated a fewer number of times so that the transmission spectra present the same passbands and banggaps of the dispersion relation spectra.

The electromagnetic wave transmission T is plotted as a function of the reduced frequency Ω (from zero to 10, corresponding to zero to $314 \text{ rad} \cdot \text{THz}$) and the incident angle θ (from 0° to 90°). In Fig. 3, we show the spectra for the sequences: (a) periodic, (b) Fibonacci, (c) Octonacci, and (d) Dodecanacci; in Fig. 4, we show the spectra for different probabilities of layer A of the random sequence, namely: (a) $p(A) = 0.2$, (b) $p(A) = 0.4$, (c) $p(A) = 0.6$, and (d) $p(A) = 0.8$. In both figures, we present results for optical multilayers with (WG) and without (WOG) graphene embedded in the structures. The color scale at the top of the figures represents magnitude of the

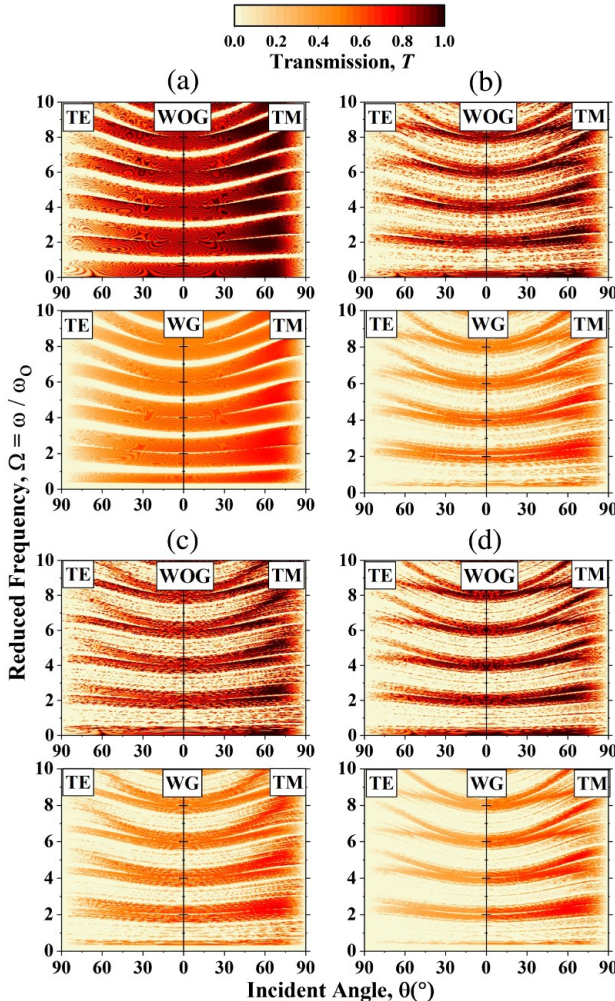


Fig. 3. Light transmission spectra for TE (left) and TM (right) obliquely incident waves propagating in 1DPC, without (WOG) and with (WG) embedded graphene sheets, for (a) periodic, (b) Fibonacci, (c) Octonacci, and (d) Dodecanacci structures.

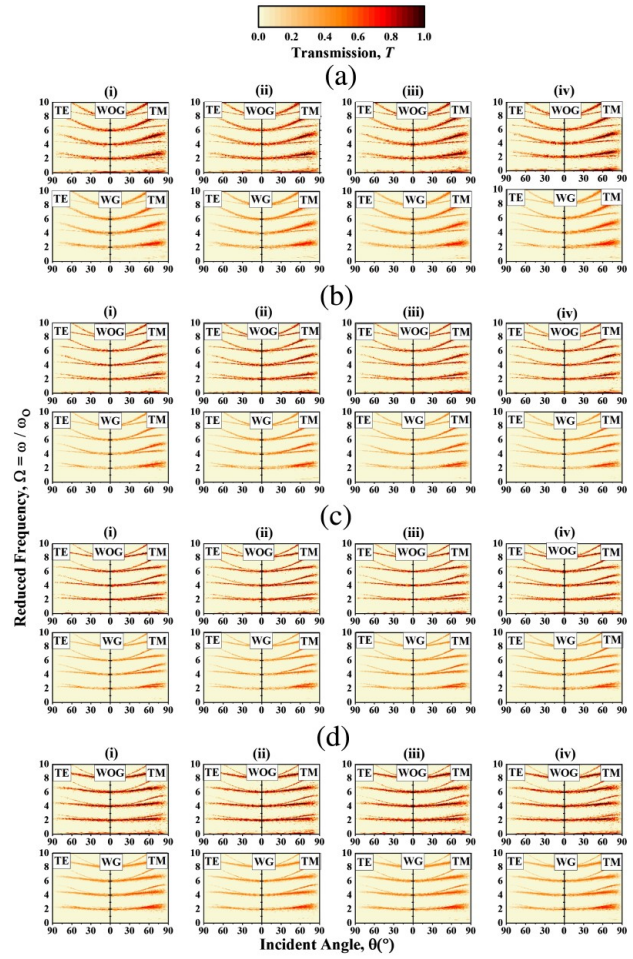


Fig. 4. Same as Fig. 3 but for a random 1DPC with $p(A)$ equal to (a) 0.2, (b) 0.4, (c) 0.6, and (d) 0.8.

light transmission coefficient on a scale from zero (bright color) to one (black color), so that regions of the plots having darker (brighter) shades represent high (low) transmission coefficients. Therefore, each point on the contour plots corresponds to a given pair composed of the angle of incidence and reduced frequency, as well as the color corresponding to the transmission coefficient magnitude. This method of visualization allows us to easily determine the PBGs occurring across the full range of angles and frequencies.

In general, it can be seen that all structures present similar spectra regarding the bandgaps and alternating patterns of dark and bright regions, which occur in both figures for all structures considered here. Interestingly, in addition to the wider bandgaps occurring at regular intervals of frequency, we also observe narrow bright regions emerging in the middle of every transmission band. These narrow PBGs occur around values of the reduced frequencies $\Omega \sim 2, 4, 6, 8$. For the WOG case, as the incident angle θ decreases, the tiny bandgaps vanish, and the light transmission does occur for $0 < \theta < 15^\circ$. In Fig. 3, considering the WG case, in the low frequency region ($\Omega \leq 0.28$, $\omega \leq 9 \text{ rad} \cdot \text{THz}$), we observe the presence of GIPBG for all values of the incident angle θ . This omnidirectional bandgap was already reported, and its physical origin is explained in Ref. [27].

Furthermore, for Ω around two, four, six, and eight, we can also observe narrow GIPBGs for normal incidence ($\theta = 0^\circ$). As a matter of fact, these narrow GIPBGs are not omnidirectional bandgaps, since they depend on the incident angle θ . For instance, in Fig. 3(a) and considering TM waves, for θ between 45° and 60° , the narrow GIPBGs around $\Omega = 2$ vanish, and transmission of the electromagnetic waves does occur. Therefore, for a range of incident angles and reduced frequency, PCs with graphene embedded display an unexpected property: the electromagnetic radiation is transmitted mainly through the multilayer and not reflected or absorbed as expected for large structures [52]. In order to take a closer look at our numerical results, we labeled the GIPBGs that emerge at $\Omega \sim 2, 4, 6, 8$ as bandgaps ①, ②, ③, ④, respectively. The numerical results are organized in Table 2 for the periodic and quasiperiodic cases corresponding to Fig. 3 for both TE and TM waves, while Tables 3 and 4 summarize the results for random sequences with data extracted from Fig. 4 for TE and TM waves, respectively.

For comparison purposes, Table 2 presents the value of the transmission coefficient for without graphene (TWOG) and with graphene (TWG) cases, considering specific values of the reduced frequencies Ω and incident angle θ within the PBGs of the graphene-free structures. Our numerical results show that, for given values of Ω and θ , the optical transmission is enhanced by the presence of graphene for all bandgaps and structures considered here. For example, the Dodecanacci case transmission increases, due to the presence of graphene, to at least 36.9%, reaching up to 76.4% (highlighted in bold and underlined in the table).

As we can observe from Table 2, those considerable gains in the transmission occur for the four bandgap regions, proving the strong influence of the graphene on the optical structures considered here. However, we should observe that for bandgaps ① and ②, the enhancement of the transmission is $\geq 55\%$, while for bandgaps ③ and ④, the enhancement of the transmission is $\leq 50\%$. The explanation for this relies on the fact the graphene optical conductivity decreases as the reduced frequency increases, thus making the influence of graphene on the propagation of the electromagnetic wave less effective [27].

After addressing PCs that follow periodic and Nacci family quasiperiodic sequences, we also investigated in our work structures whose constituent elements A and B are arranged according to random sequences generated via a given value of $p(A)$, which is the occurrence probability of the material A in the structure. For instance, for $p(A) = 0.2$, we have 20% of A layers and 80% of B layers; for $p(A) = 0.4$, we have 40% of A layers and 60% of B layers; for $p(A) = 0.6$ and 0.8 , we have 60% of A layers and 40% of B layers, and 80% of A layers and 20% of B layers, respectively. Also, for each value of $p(A)$, we have considered four different random sequences and labeled them as (i), (ii), (iii), and (iv).

The numerical results for 1DRPC are plotted in Fig. 4, from which we can observe a pattern of the contour plots similar to those in Fig. 3, but with the brighter regions dominating, with broad bandgaps and narrow transmission bands, which means that the transmissivity is lower for random structures compared to the periodic and quasiperiodic arrangements. In fact, a random arrangement of the structure makes difficult the electromagnetic waves propagation [53]. Also, unlike the results

Table 2. Transmission Values for PC and PQC^a

	Ω	Bandgap ①			Bandgap ②			Bandgap ③			Bandgap ④			
		θ ($^\circ$)	TWOG	TWG	θ ($^\circ$)	TWOG	TWG	θ ($^\circ$)	TWOG	TWG	θ ($^\circ$)	TWOG	TWG	
TE	Periodic	2.19	45	0	0.592	4.12	24	0	0.606	6.08	16	0	0.497	8.05
	Fibonacci	2.22	47	0	0.577	4.12	24	0	0.550	6.09	16	0	0.553	8.05
	Octonacci	2.17	47	0	0.621	4.10	25	0	0.589	6.06	15	0	0.493	8.04
	Dodecanacci	2.30	52	0	0.369	4.18	27	0	0.640	6.12	18	0	0.510	8.07
TM	Periodic	2.19	45	0	0.614	4.12	24	0	0.627	6.08	16	0	0.524	8.05
	Fibonacci	2.22	47	0	0.648	4.12	24	0	0.538	6.09	16	0	0.545	8.05
	Octonacci	2.17	47	0	0.550	4.10	25	0	0.533	6.06	15	0	0.429	8.04
	Dodecanacci	2.30	52	0	0.764	4.18	27	0	0.664	6.12	18	0	0.547	8.07

^aHere Ω , TWOG, and TWG mean reduced frequency, transmission without graphene, and transmission with graphene, respectively (see Fig. 3).

presented in Fig. 3, the bandgap widths in random sequences increase as the incident angle increases, even for TM waves, for which the bandgaps slowly increase, and, for the region around $\Omega = 2$ and $\theta = 60^\circ$, they even get closed. Furthermore, it is very interesting that even in these non-deterministic cases, PBGs occur around the same reduced frequencies, i.e., $\Omega = 2, 4, 6, 8$. This is a consequence of the strong influence of the quarter-wavelength condition employed to design the slabs thicknesses [54].

Similar to the periodic and quasiperiodic cases, the transmission is enhanced within the bandgaps when graphene is embedded in the multilayer. As this statement is not so easy to see in Fig. 4, the data proving the occurrence of this phenomenon in random sequences are presented and organized in Table 3, for TE waves, and Table 4, for TM waves. For example, for given values of Ω and θ , the enhancement of the transmission for TE waves is $\geq 22\%$ and $\leq 61.9\%$; for TM waves, the enhancement of the transmission is $\geq 20.8\%$ and $\leq 74.7\%$.

Table 3. Same as Table 2, but for 1DRPC and TE Polarization (see Fig. 4)

		Bandgap ①				Bandgap ②				Bandgap ③				Bandgap ④			
		Ω	θ ($^\circ$)	TWOG	TWG	Ω	θ ($^\circ$)	TWOG	TWG	Ω	θ ($^\circ$)	TWOG	TWG	Ω	θ ($^\circ$)	TWOG	TWG
TE waves	i	2.20	50	0	0.544	4.11	28	0	0.337	6.08	19	0	0.354	8.07	15	0	0.363
		2.20	50	0.0038	0.542	4.11	28	0	0.222	6.08	19	0	0.482	8.07	15	0	0.363
		2.20	50	0.0021	0.569	4.11	28	0	0.362	6.08	19	0	0.373	8.07	15	0	0.404
		2.20	50	0	0.533	4.11	28	0	0.403	6.08	19	0	0.392	8.07	15	0	0.349
	ii	2.19	47	0	0.421	4.11	24	0	0.595	6.09	18	0	0.358	8.08	15	0	0.223
		2.19	47	0	0.418	4.11	24	0	0.619	6.09	18	0	0.487	8.08	15	0	0.389
		2.19	47	0	0.424	4.11	24	0	0.609	6.09	18	0	0.416	8.08	15	0	0.336
		2.19	47	0	0.428	4.11	24	0	0.596	6.09	18	0	0.445	8.08	15	0	0.392
	iii	2.21	45	0	0.351	4.13	24	0	0.595	6.11	18	0	0.197	8.08	14	0	0.491
		2.21	45	0	0.360	4.13	24	0	0.564	6.11	18	0	0.277	8.08	14	0.0030	0.420
		2.21	45	0	0.382	4.13	24	0	0.592	6.11	18	0	0.322	8.08	14	0	0.487
		2.21	45	0	0.371	4.13	24	0	0.591	6.11	18	0	0.293	8.08	14	0.0012	0.435
	iv	2.35	55	0	0.452	4.22	30	0	0.321	6.15	20	0	0.475	8.10	14	0	0.441
		2.35	55	0	0.220	4.22	30	0	0.460	6.15	20	0	0.482	8.10	14	0	0.438
		2.35	55	0	0.228	4.22	30	0	0.461	6.15	20	0	0.557	8.10	14	0	0.450
		2.36	55	0	0.580	4.22	30	0	0.361	6.15	20	0	0.561	8.10	14	0	0.407

Table 4. Same as Table 2, but for 1DRPC and TM Polarization (see Fig. 4)

		Bandgap ①				Bandgap ②				Bandgap ③				Bandgap ④			
		Ω	θ ($^\circ$)	TWOG	TWG	Ω	θ ($^\circ$)	TWOG	TWG	Ω	θ ($^\circ$)	TWOG	TWG	Ω	θ ($^\circ$)	TWOG	TWG
TM waves	i	2.17	52	0	0.323	4.11	28	0	0.448	6.08	19	0	0.403	8.07	15	0	0.396
		2.17	52	0	0.280	4.11	28	0	0.270	6.08	19	0	0.545	8.07	15	0	0.395
		2.17	51	0	0.306	4.11	28	0	0.448	6.08	19	0	0.417	8.07	15	0	0.435
		2.17	52	0	0.208	4.11	28	0	0.424	6.08	19	0	0.437	8.07	15	0	0.386
	ii	2.19	47	0	0.616	4.11	24	0	0.586	6.09	18	0	0.423	8.07	14	0	0.407
		2.19	47	0	0.724	4.11	24	0	0.576	6.09	18	0	0.520	8.08	15	0	0.413
		2.19	47	0	0.731	4.11	24	0	0.590	6.09	18	0	0.457	8.08	15	0	0.362
		2.19	47	0	0.629	4.11	24	0	0.606	6.09	18	0	0.476	8.08	15	0	0.417
	iii	2.21	45	0	0.657	4.13	24	0	0.640	6.10	18	0	0.535	8.08	14	0.0019	0.504
		2.21	45	0	0.719	4.13	24	0	0.635	6.10	18	0	0.530	8.08	14	0.0058	0.439
		2.21	45	0	0.741	4.13	24	0	0.649	6.10	18	0	0.540	8.08	14	0.0021	0.501
		2.21	45	0	0.666	4.13	24	0	0.662	6.10	18	0	0.562	8.08	14	0.0031	0.453
	iv	2.35	55	0	0.716	4.22	30	0	0.493	6.15	20	0	0.489	8.10	14	0	0.459
		2.35	55	0	0.740	4.22	30	0	0.654	6.15	20	0	0.514	8.10	14	0	0.458
		2.35	55	0	0.717	4.22	30	0	0.570	6.15	20	0	0.573	8.10	14	0	0.470
		2.35	55	0	0.747	4.22	30	0	0.573	6.15	20	0	0.582	8.10	14	0	0.433

Those values are highlighted in bold and underlined in Tables 3 and 4. As expected, the enhancement of the transmission is higher for TM than TE waves considering the same random structure for a given value of $p(A)$. Also, the enhancement occurs around the bandgaps ①, ②, ③, and ④, for the four different random structures considering a given probability $p(A)$. As before, those numerical results confirm the strong influence of the graphene presence on the bandgaps and transmission spectra of the optical structures considered here. However, for random sequences, the enhancement of the transmission is, in most cases, below 50% for TE waves (despite the bandgap region and the probability $p(A)$), while for TM waves, the enhancement of the transmission is above 50%, in most cases, with $p(A) \geq 0.4$, especially in bandgap ①, for which the influence of the graphene optical conductivity is stronger.

Finally, we should remark that for $p(A) = 0.8$, the enhancement of the transmission is above 70% for all random structures investigated. This is a very interesting result and makes these structures very useful for applications, as logical gates or sensors based on PCs, by controlling the number of building layers A (which in our work corresponds to SiO_2) [55].

Surely our model can be realized experimentally, although some difficulties may exist. On one hand, fabrication of graphene monolayers and transfer onto different substrates is a feasible task, for instance, by exfoliation and chemical methods [56]. On the other hand, the alternation of sputtering SiO_2 and TiO_2 layers combined with graphene monolayer transfer can be a tough task. This can be a challenging experimental work, and we hope that experimentalists are encouraged to face it.

4. CONCLUSION

In summary, we have employed a transfer-matrix treatment to study the propagation of electromagnetic waves in 1DPCs made of two different dielectric slabs (silicon dioxide and titanium dioxide) separated by graphene. The structures considered in this work are spatially arranged according to periodic sequence, quasiperiodic Nacci family sequences (Fibonacci, Octonacci, and Dodecanacci), and also random sequences. We calculated their transmission spectra as a function of incident angle θ and reduced frequency Ω . Our main goal was to investigate the enhancement of the transmission due to the presence of graphene. Our numerical results show a diversity of stop and pass photonic bands. Regarding the polarization of the light wave, we can observe in Figs. 3 and 4 that the transmission coefficient is higher for the TM case than for the TE case, as expected. In particular, we show that bandgap regions become passband regions when graphene is embedded in the optical multilayer. More specifically, for a range of incident angles and reduced frequency, the PCs with graphene embedded display an unexpected property: the electromagnetic radiation is transmitted through the multilayers and not absorbed as expected for large structures. The enhancement of the transmission for periodic and quasiperiodic cases is, in most cases, at least $\geq 50\%$, reaching up to $\geq 76.4\%$. While for the random cases, the transmission is enhanced, in most cases, at least $\geq 50\%$, reaching up to $\geq 76.4\%$.

Funding. Brazilian Research Agencies CNPq (429299/2016-8, 310561/2017-5); FUNCAP (BP3-0139-00177.01.00/18). 2 390

Disclosures. The authors declare no conflicts of interest. 391

REFERENCES

1. E. Yablonovitch, "Inhibited spontaneous emission in solid-state physics and electronics," *Phys. Rev. Lett.* **58**, 2059 (1987). 393
2. S. John, "Strong localization of photons in certain disordered dielectric superlattices," *Phys. Rev. Lett.* **58**, 2486 (1987). 394
3. N. Kumar and B. Suthar, eds., *Advances in Photonic Crystals and Devices*, 1st ed. (CRC Press, 2019). 395
4. W. Jin, M. Song, X. Yue, and Y. Gao, "Optical induced area-controllable two-dimensional eight-fold symmetric photonic quasicrystal microstructures," *Opt. Mater.* **100**, 109719 (2020). 396
5. J. Liu, W. Tan, E. Liu, H. Hu, Z. Fan, T. Zhang, and X. Zhang, "Planar scanning method for detecting refraction characteristics of two-dimensional photonic quasi-crystal wedge-shaped prisms," *J. Opt. Soc. Am. A* **33**, 978–983 (2016). 397
6. B. Feng, E. Liu, Z. Wang, W. Cai, H. Liu, S. Wang, T. Liang, W. Xiao, and J. Liu, "Generation of terahertz hollow beams by a photonic quasi-crystal flat lens," *Appl. Phys. Express* **9**, 062003 (2016). 398
7. W. Tan, E. Liu, B. Yan, J. Xie, R. Ge, D. Tang, J. Liu, and S. Wen, "Subwavelength focusing of a cylindrically symmetric plano-concave lens based on a one-dimensional Thue–Morse photonic quasicrystal," *Appl. Phys. Express* **11**, 092002 (2018). 399
8. W. Zhang, W. Tan, Q. Yang, T. Zhou, and J. Liu, "Subwavelength focusing in visible light band by a Fibonacci photonic quasi-crystal plano-concave lens," *J. Opt. Soc. Am. B* **35**, 2364–2367 (2018). 400
9. H. Zhao, J. Xie, and J. Liu, "An approximate theoretical explanation for super-resolution imaging of two-dimensional photonic quasi-crystal flat lens," *Appl. Phys. Express* **13**, 022007 (2020). 401
10. Y. Zhao, Z. Wang, Z. Jiang, C. Yue, X. Chen, J. Wang, and J. Liu, "Add-drop filter with compound structures of photonic crystal and photonic quasicrystal," *J. Infrared Millim. Terahertz Waves* **36**, 342 (2017). 402
11. J. Ren, X. Sun, and S. Wang, "A narrowband filter based on 2D 8-fold photonic quasicrystal," *Superlattices Microst.* **116**, 221 (2018). 403
12. E. Liu, W. Tan, B. Yan, J. Xie, R. Ge, and J. Liu, "Broadband ultra-flattened dispersion, ultra-low confinement loss and large effective mode area in an octagonal photonic quasi-crystal fiber," *J. Opt. Soc. Am. A* **35**, 431–436 (2018). 404
13. Q. Liu, B. Yan, and J. Liu, "U-shaped photonic quasi-crystal fiber sensor with high sensitivity based on surface plasmon resonance," *Appl. Phys. Express* **12**, 052014 (2019). 405
14. E. Liu, S. Liang, and J. Liu, "Double-cladding structure dependence of guiding characteristics in six-fold symmetric photonic quasi-crystal fiber," *Superlattices Microst.* **130**, 61 (2019). 406
15. E. Liu, W. Tan, B. Yan, J. Xie, R. Ge, and J. Liu, "Robust transmission of orbital angular momentum mode based on a dual-cladding photonic quasi-crystal fiber," *J. Phys. D* **52**, 325110 (2019). 407
16. Q. Liu, J. Sun, Y. Sun, W. Liu, F. Wang, L. Yang, C. Liu, Q. Liu, Q. Li, Z. Ren, T. Sun, and P. K. Chu, "Surface plasmon resonance sensor based on eccentric core photonic quasi-crystal fiber with indium tin oxide," *Appl. Opt.* **58**, 6848 (2019). 408
17. Z. Huo, E. Liu, and J. Liu, "Hollow-core photonic quasicrystal fiber with high birefringence and ultra-low nonlinearity," *Chin. Opt. Lett.* **18**, 030603 (2020). 409
18. Q. Liu, Z. Ren, Y. Sun, Q. Liu, W. Liu, C. Liu, J. Sun, Q. Li, T. Sun, and P. K. Chu, "Numerical analysis of a high-birefringent photonic quasi-crystal fiber with circular air holes," *Optik* **207**, 163850 (2020). 410
19. A. Shi, R. Ge, and J. Liu, "Refractive index sensor based on photonic quasi-crystal with concentric ring microcavity," *Superlattices Microst.* **133**, 106198 (2019). 411
20. Y. Tang, J. Deng, K. Li, M. Jin, J. Ng, and G. Li, "Quasicrystal photonic metasurfaces for radiation controlling of second harmonic generation," *Adv. Mater.* **31**, 1901188 (2019). 412

- 454
455 21. Y. An, Z. Gao, and Z. Ouyang, "Surface wave photonic quasicrystal,"
456 *Appl. Phys. Lett.* **116**, 151104 (2020).
457 22. C. Yue, W. Tan, and J. Liu, "Photonic band gap properties of one-
458 dimensional Thue-Morse all-dielectric photonic quasicrystal,"
459 *Superlattices Microst.* **117**, 252 (2018).
460 23. Y. Trabelsi, N. Ben Ali, W. Belkadj, and M. Kanzari, "Photonic band
461 gap properties of one-dimensional generalized Fibonacci photonic
462 quasicrystal containing superconductor material," *J. Supercond. Nov. Magn.* **32**, 3541 (2019).
463 24. B. E. A. Saleh and M. C. Teich, *Fundamentals of Photonics*, 3rd ed.
464 (Wiley, 2019).
465 25. K. Yasumoto, ed., *Electromagnetic Theory and Applications for*
466 *Photonic Crystals*, 1st ed. (CRC Press, 2018).
467 26. T. J. Cui, D. Smith, and R. Liu, eds., *Metamaterials: Theory, Design,*
468 *and Applications*, 1st ed. (Springer, 2014).
469 27. C. H. Costa, L. F. C. Pereira, and C. G. Bezerra, "Light propagation in
470 quasiperiodic dielectric multilayers separated by graphene," *Phys. Rev. B* **96**,
471 125412 (2017).
472 28. D. Shechtman, I. Blech, D. Gratias, and J. W. Cahn, "Metallic phase
473 with long-range orientational order and no translational symmetry,"
474 *Phys. Rev. Lett.* **53**, 1951 (1984).
475 29. C. G. Bezerra, E. L. Albuquerque, A. M. Mariz, L. R. da Silva, and
476 C. Tsallis, "Spin wave specific heat in quasiperiodic Fibonacci
477 structures," *Physica A* **294**, 415 (2001).
478 30. I. P. Coelho, M. S. Vasconcelos, and C. G. Bezerra, "Effects of mirror
479 symmetry on the transmission fingerprints of quasiperiodic photonic
480 multilayers," *Phys. Lett. A* **374**, 1574 (2010).
481 31. C. Janot, *Quasicrystals: A Primer* (Oxford University, 2012).
482 32. A. N. Poddubny and E. L. Ivchenko, "Photonic quasicrystalline and
483 aperiodic structures," *Physica E* **42**, 1871 (2010).
484 33. Z. V. Vardeny, A. Nahata, and A. Agrawal, "Optics of photonic
485 quasicrystals," *Nature Photonics* **7**, 177–187 (2013).
486 34. C. Nayak, C. H. Costa, and A. Aghajamali, "Robust photonic
487 bandgaps in quasiperiodic and random extrinsic magnetized
488 plasma," *IEEE Trans. Plasma Sci.* **47**, 1726 (2019).
489 35. C. Nayak, A. Aghajamali, F. Scotognella, and A. Saha, "Effect of
490 standard deviation, strength of magnetic field and electron density
491 on the photonic band gap of an extrinsic disorder plasma photonic
492 structure," *Opt. Mater.* **72**, 25 (2017).
493 36. T. Yuan, T. Feng, and Y. Xu, "Manipulation of transmission by engi-
494 neered disorder in one-dimensional photonic crystals," *Opt. Express*
495 **27**, 6483–6494 (2019).
496 37. C. Nayak, C. H. Costa, and K. V. P. Kumar, "Photonic bandgap of
497 random in layer position extrinsic magnetized plasma multilayer,"
498 *IEEE Trans. Plasma Sci.* (to be published).
499 38. Y. Wu, J. Zhu, and L. Huang, "A review of three-dimensional
500 graphene-based materials: synthesis and applications to energy
501 conversion/storage and environment," *Carbon* **143**, 610 (2019).
502 39. S. Zhang, Z. Li, and F. Xing, "Review of polarization optical devices
503 based on graphene materials," *Int. J. Mol. Sci.* **21**, 1608 (2020).
504 40. Q. Bao and K. P. Loh, "Graphene photonics, plasmonics, and broad-
505 band optoelectronic devices," *ACS Nano* **6**, 3677 (2012).
506 41. F. J. Garcia de Abajo, "Graphene nanophotonics," *Science* **339**,
507 917–918 (2013).
508 42. P. Tassin, T. Koschny, and C. M. Soukoulis, "Graphene for terahertz
509 applications," *Science* **341**, 620–621 (2013).
510 43. Y. Wang, "Transfer matrix theory of monolayer graphene/bilayer
511 graphene heterostructure superlattice," *J. Appl. Phys.* **116**, 164317
512 (2014).
513 44. C. Nayak, A. Aghajamali, T. Alamfard, and A. Saha, "Tunable photonic
514 band gaps in an extrinsic Octonacci magnetized cold plasma quasi-
515 crystal," *Physica B* **525**, 41 (2017).
516 45. C. Nayak, "Dodecanacci extrinsic magnetized plasma multilayer,"
517 *Opt. Mater.* **100**, 109653 (2020).
518 46. I. M. Felix and L. F. C. Pereira, "Suppression of coherent thermal
519 transport in quasiperiodic graphene-hBN superlattice ribbons,"
520 *Carbon* **160**, 335 (2020).
521 47. S. Mehdi, G. Mahboubeh, and L. Leila, "Donor impurity effects
522 on optical properties of GaN/AlN constant total effective radius
523 multishell quantum dots," *J. Opt. Soc. Am. B* **33**, 420–425 (2016).
524 48. M. Aliofkhazraei, N. Ali, W. I. Milne, C. S. Ozkan, S. Mitura, and J. L.
525 Gervasoni, eds., *Graphene Science Handbook: Electrical and Optical*
526 *Properties* (CRC Press, Boca Raton, 2016).
527 49. A. Madani and S. R. Entezar, "Optical properties of one-dimensional
528 photonic crystals containing graphene sheets," *Physica B* **431**, 1
529 (2013).
530 50. R. Luck, "Basic ideas of Ammann bar grids," *Int. J. Mod. Phys. B* **7**,
531 1437 (1993).
532 51. C. H. O. Costa and M. S. Vasconcelos, "Band gaps and transmission
533 spectra in generalized Fibonacci $\sigma(p,q)$ one-dimensional magnonic
534 quasicrystals," *J. Phys. Condens. Matter* **25**, 286002 (2013).
535 52. E. F. Silva, C. Costa, M. S. Vasconcelos, and D. H. A. L. Anselmo,
536 "Transmission spectra in graphene-based Octonacci one-
537 dimensional photonic quasicrystals," *Opt. Mater.* **89**, 623
538 (2019).
539 53. M. Ghulinyan and L. Pavesi, eds., *Light Localisation and Lasing:*
540 *Random and Quasi-Random Photonic Structures* (Cambridge
541 University, 2014).
542 54. Y. Fan, Z. Wei, H. Li, H. Chen, and C. M. Soukoulis, "Photonic band
543 gap of a graphene-embedded quarter-wave stack," *Phys. Rev. B* **88**,
544 241403 (2013).
545 55. M. F. O. Hameed and S. Obayya, eds., *Computational Photonic*
546 *Sensors* (Springer, 2019).
547 56. H. C. Lee, W.-W. Liu, S.-P. Chai, A. R. Mohamed, A. Aziz, C.-S. Khe,
548 N. M. S. Hidayah, and U. Hashim, "Review of the synthesis, transfer,
549 characterization and growth mechanisms of single and multilayer
550 graphene," *RSC Adv.* **7**, 15644 (2017).

Queries

1. AU: Please check and confirm the edit made in the article title.
2. AU: The funding information for this article has been generated using the information you provided to OSA at the time of article submission. Please check it carefully. If any information needs to be corrected or added, please provide the full name of the funding organization/institution as provided in the CrossRef Open Funder Registry (<https://search.crossref.org/funding>).